AD-A169 611 CALCULATION OF POTENTIAL ENERGY SURFACES FOR HCO AND HNO USING MANY-BODY METHODS(U) ARMY BALLISTIC RESEARCH LAB ABERDEEN PROVING GROUND MD G F ADAMS ET AL. JUN 86 1/1

UNCLASSIFIED BRL-TR-2737 F/G 7/4 NL

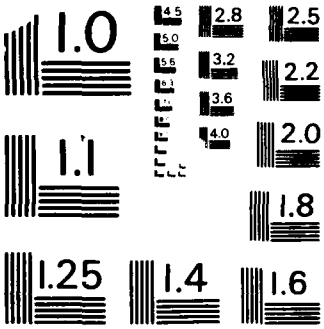

MICROCOPY RESOLUTION TEST CHART

NATIONAL BUREAU OF STANDARDS - 1963 - A

US ARMY
MATERIEL
COMMAND

AD

(12)

TECHNICAL REPORT BRL-TR-2737

AD-A169 611

CALCULATION OF POTENTIAL ENERGY SURFACES FOR HCO AND HNO USING MANY-BODY METHODS

George F. Adams
Gary D. Bent

DTIC
ELECTE
JUL 7 1986
A

June 1986

APPROVED FOR PUBLIC RELEASE; DISTRIBUTION UNLIMITED.

US ARMY BALLISTIC RESEARCH LABORATORY
ABERDEEN PROVING GROUND, MARYLAND

DTIC FILE COPY

86

Destroy this report when it is no longer needed.
Do not return it to the originator.

Additional copies of this report may be obtained from the National Technical Information Service, U. S. Department of Commerce, Springfield, Virginia 22161.

The findings in this report are not to be construed as an official Department of the Army position, unless so designated by other authorized documents.

The use of trade names or manufacturers' names in this report does not constitute indorsement of any commercial product.

UNCLASSIFIED

SECURITY CLASSIFICATION OF THIS PAGE (When Data Entered)

REPORT DOCUMENTATION PAGE

READ INSTRUCTIONS BEFORE COMPLETING FORM

1. REPORT NUMBER: Technical Report BRL-TR-2737

2. GOVT ACCESSION NO.: AD-A169611

3. RECIPIENT'S CATALOG NUMBER:

4. TITLE (and Subtitle): CALCULATION OF POTENTIAL ENERGY SURFACES FOR HCO AND HNO USING MANY-BODY METHODS

5. TYPE OF REPORT & PERIOD COVERED: Final

6. PERFORMING ORG. REPORT NUMBER:

7. AUTHOR(s):

George F. Adams
Gary D. Bent*

8. CONTRACT OR GRANT NUMBER(s):

9. PERFORMING ORGANIZATION NAME AND ADDRESS:

US Army Ballistic Research Laboratory
ATTN: SLCBR-IB
Aberdeen Proving Ground, MD 21005-5066

10. PROGRAM ELEMENT, PROJECT, TASK AREA & WORK UNIT NUMBERS: 1L161102AH43

11. CONTROLLING OFFICE NAME AND ADDRESS:

U.S. Army Ballistic Research Laboratory
ATTN: SLCBR-DD-T
Aberdeen Proving Ground, MD 21005-5066

12. REPORT DATE: June 1986

13. NUMBER OF PAGES: 46

14. MONITORING AGENCY NAME & ADDRESS (if different from Controlling Office):

15. SECURITY CLASS. (of this report): Unclassified

15a. DECLASSIFICATION/DOWNGRADING SCHEDULE: NA

16. DISTRIBUTION STATEMENT (of this Report)

Approved for Public Release; Distribution Unlimited.

17. DISTRIBUTION STATEMENT (of the abstract entered in Block 20, if different from Report)

18. SUPPLEMENTARY NOTES

*University of Connecticut
Storrs, CT

19. KEY WORDS (Continue on reverse side if necessary and identify by block number)

Many-Body Perturbation Theory
Formyl Radical
Hydrogen Nitroxide
Unimolecular Reaction

20. ABSTRACT (Continue on reverse side if necessary and identify by block number) meg

Many-body perturbation theory calculations of the potential energy surfaces pertinent to the hydrogen dissociation reaction of the ground state of the formyl radical and the three lowest electronic states of hydrogen nitroxide are summarized. The calculations established that MBPT provides a reasonable description of the reaction pathway for those molecules not requiring a multiconfiguration zeroth order wavefunction. The data obtained for the three states of HNO provide the basis for a statistical estimate of

DD FORM 1 JAN 73 1473 EDITION OF 1 NOV 65 IS OBSOLETE

UNCLASSIFIED

SECURITY CLASSIFICATION OF THIS PAGE (When Data Entered)

20. Abstract (Cont'd):

relative recombination rates in production of these states, leading to a plausible identification of the source of the chemiluminescence that characterizes this chemical species. Keywords:

Cont'd DD 1473

TABLE OF CONTENTS

Page

LIST OF TABLES.....5

I. INTRODUCTION.....7

II. OUTLINE OF THEORY AND COMPUTATIONS.....7

III. GROUND STATE POTENTIAL ENERGY SURFACE FOR THE FORMYL RADICAL...12

A. Background.....12
B. Potential Energy Surface for HCO + M → H + CO + M.....13

IV. POTENTIAL ENERGY SURFACES FOR DISSOCIATION OF HYDROGEN NITROXIDE, HNO.....18

A. Background.....18
B. Predicted Structures.....19
C. Excitation Energies.....19
D. Potential Energy Curves for Hydrogen Dissociation Reactions of HNO.....23
E. Relative Rates for Recombination Into Three Electronic States of HNO.....27

V. DISCUSSION.....30

ACKNOWLEDGMENT.....33

REFERENCES.....35

DISTRIBUTION LIST.....41

QUALITY INSPECTED 1

Accession For
NTIS GRA&I
DTIC TAB
Unannounced
Justification
By
Distribution/
Availability Codes
Avail and/or
Dist Special
A-1

LIST OF TABLES

Table		Page
1	Structural Parameters for Formyl Radical, HCO	13
2	Empirical and Theoretical Values of Dissociation Energy for HCO	14
3	Energy of HCO for Selected R_{CH} and Classical Barrier Height and Dissociation Energy at Several Levels of Calculation	15
4	Vibrational Frequencies (cm^{-1}) for HCO and the Transition State for the Dissociation Reaction	17
5	Comparison of Predicted and Experimental Structural Parameters for HNO and NO	20
6	Electronic Energy Predictions for Equilibrium Structures of HNO	21
7	Vibrational Frequencies of HNO	22
8	Adiabatic Excitation Energies (kcal/mol) for HNO	23
9	Dissociation Energies of HNO	24
10	Electronic Energy Predictions for HNO at Selected Values of R_{NH} for Each State and Classical Dissociation Energy and Barrier Height for Each State	25
11	Molecular Data for Hydrogen Nitroxide (cm^{-1}, amu $Å^2$, kcal/mol)	29
12	Low Pressure Rate Coefficients and Equilibrium Constant Ratios for HNO, T = 300 K	30

I. INTRODUCTION

It has been recognized, since the work of Eyring and Polanyi,[1] that an understanding of detailed reaction dynamics requires a knowledge of the topographical features of the potential energy hypersurfaces pertinent to the chemical reaction. The task of the theoretician is to refine electronic structure calculations so that electronic energy differences on an energy surface may be predicted with "chemical accuracy," or about 2 kcal/mol. Recent publications, by several different groups, establish the importance of electron correlation effects in studying even qualitative aspects of potential energy surfaces,[2-5] and experience to date indicates that neglect of the effects of electron correlation can lead to substantial errors in predicted heats of reaction.

In previous publications we have described the application of the linked-diagram-based methods, many-body perturbation theory and coupled-cluster double-excitation theory, for the computation of potential energy surfaces,[3] electronic excitation energies,[5,6] and molecular properties.[5] Here we report details of potential energy surface features for two species commonly found in flames: formyl radical, HCO, and hydrogen nitroxide, HNO. In particular, we consider the hydrogen dissociation reactions of these species:

$$HCO(X^1A') \rightarrow H(^2S) + CO(X^1\Sigma_g^+) \qquad (R1)$$

$$HNO(X^1A') \rightarrow H(^2S) + NO(^2\Pi) \qquad (R2)$$

$$HNO(a^3A'') \rightarrow H(^2S) + NO(^2\Pi) \qquad (R3)$$

$$HNO(A^1A'') \rightarrow H(^2S) + NO(^2\Pi) \qquad (R4)$$

Detailed results will be presented for the potential surfaces pertinent to these four reactions. In particular, we have computed the minimum-energy pathways. A less complete description of the formyl radical potential energy surface has appeared previously.[3]

Each of the potential energy surfaces to be described in this report pertains to a reaction important in flames. In particular, reactions (R1)-(R4) promise to be important in the oxidation of formaldehyde by nitrogen dioxide.[7]

In the following section we present an overview of the theoretical calculations. The succeeding sections report reaction hypersurfaces for each of the chemical species. In the case of hydrogen nitroxide, we also report simplified rate coefficient estimates in a discussion of the recombination of hydrogen and nitrogen oxide.

II. OUTLINE OF THEORY AND COMPUTATIONS

Many-body perturbation theory (MBPT)[8-10] and coupled-cluster methods (CCM)[11-14] are relatively new techniques, compared to configuration interaction (CI), for the determination of electron correlation effects on potential energy surfaces.[3,5,6,14-25] MBPT/CCM methods were orginally developed for problems in nuclear and solid state physics,[8,9] where emphasis

on correct size dependence, which we refer to as "size extensivity," is mandatory. Size extensivity is guaranteed by the evaluation of terms that the many-body formalism identifies as linked-diagrams,[9] hence, the linked-diagram theorem serves as the cornerstone of the theory. In a solid of an infinite number of atoms, the correct size dependence is obviously crucial, yet even in molecular problems this is a highly desirable trait for an approximate method to possess.[5,14] Two primary reasons for this are: (a) only approximate methods that scale properly with size are suitable for generalization to larger molecules, such as those encountered in quantum biochemistry,[26] and (b) size extensivity assists in computing accurate dissociation energies (or, more generally, correct relative energies on the surface) when it is necessary to compare a molecule to its smaller fragments.[5] The latter kind of comparison is also crucially dependent upon basis set effects[27] and whether the approximate method permits smooth dissociation into the different components.[20] Heats of formation obtained from calculations using size-extensive methods can be used just like experimental values to obtain the heat-of-formation of some complex molecule, while non-size-extensive methods may require "supermolecule" calculations to provide accurate estimates of these quantities.[5]

MBPT/CCM can be developed from the coupled-cluster ansatz,[11-13]

$$\psi = \exp(T)|\phi_0\rangle \tag{1}$$

where

$$T = T_1 + T_2 + \ldots + T_n + \ldots \tag{2}$$

$$T_n = 1/n! \sum_{\substack{ijk\ldots \\ abc\ldots}} t_{ijk\ldots}^{abc\ldots} X_a^\dagger X_b^\dagger X_c^\dagger \cdots X_k X_j X_i \tag{3}$$

with

$$\{t_{ijk\ldots}^{abc\ldots}\}$$

the amplitudes of the n-particle second-quantized operator of Eq. (3). The form of the wavefunction in (1), combined with the condition that the T operator in (2) contains no disconnected parts, is sufficient to guarantee that the energy

$$E = \langle\phi_0|H \exp(T)|\phi_0\rangle \tag{4}$$

contains only linked vacuum diagrams and is necessarily size extensive. The common choice for ϕ_0 is a SCF function of the restricted or unrestricted form, although this is not necessary.

If we limit T to only double excitations, we obtain the coupled-cluster doubles (CCD) model.[21] Equations for the amplitudes can be obtained by back-projecting, $H \exp(T_2)|\phi_0\rangle$, onto the space of CI double excitations. This leads to a set of nonlinear coupled equations for the amplitudes:[12]

$$\langle ab||ij\rangle - D_{ijab}t_{ij}^{ab} + \sum_{c>d} \langle ab||cd\rangle t_{ij}^{cd} + \sum_{k>l} \langle kl||ij\rangle t_{kl}^{ab}$$

$$+ \sum_{k,c} (-\langle kb||jc\rangle t_{ik}^{ac} + \langle ka||jc\rangle t_{ik}^{bc} + \langle kb||ic\rangle t_{ik}^{ac}$$

$$- \langle ka||jc\rangle t_{jk}^{bc}) + \sum_{\substack{k>l \\ c>d}} \{\langle kl||cd\rangle [t_{ij}^{cd}t_{kl}^{ab} - 2(t_{ij}^{ac}t_{kl}^{bd}$$

$$+ t_{ij}^{bd}t_{kl}^{ac}) - 2(t_{ik}^{ab}t_{jl}^{cd} + t_{ik}^{cd}t_{jl}^{ab}) + 4(t_{ik}^{ac}t_{jl}^{bd} + t_{ik}^{bd}t_{jl}^{ac})]\}$$

$$= 0 \tag{5}$$

where $\langle pq||rs\rangle$ and D_{ijab} are defined in terms of SCF orbital energies ε_i and by two-electron integrals in the molecular basis set

$$\langle pq||rs\rangle = (X_pX_r|X_qX_s) - (X_pX_s|X_qX_r) \tag{6a}$$

$$(X_pX_r|X_qX_s) = \iint d\bar{r}_1\, d\bar{r}_2\, X_p^*(\bar{r}_1)\, X_r(\bar{r}_1)\, X_q^*(\bar{r}_2)\, X_s(\bar{r}_2) \tag{6b}$$

and

$$D_{ijab} = \varepsilon_i + \varepsilon_j - \varepsilon_a - \varepsilon_b \tag{6c}$$

From the number of operators involved, the highest terms in the exponential expansion that contribute to these amplitudes are quadratic.

Notice that there are no more amplitudes to determine in ψ_{CCD} than in the standard doubles-configuration-interaction (D-CI) function, yet we now have a size-extensive method that includes most of the effects of CI quadruple excitations. The latter fact follows by comparison to a CI wavefunction including quadruples since the CI quadruple-excitation operation C_4 is equivalent to

$$C_4 = T_4 + 1/2T_2^2 + 1/2T_1^2\, T_2 + T_1T_3 + \frac{1}{4!}\, T_1^4 \tag{7}$$

However, as Sinanoglu observed,[23] T_4, which accounts for true four-particle interactions, is very small, while T_2^2, which accounts for two simultaneous two-particle interactions, is far more important. Also $T_1 = 0$ for Brueckner orbitals, and it is usually small for SCF orbitals, so the last three terms are normally unimportant. Hence, with only little more effort than required for D-CI, we obtain a substantially better result.

The iterative solution of Eq. (5) proceeds as follows. Initially the nonlinear term is neglected, giving

$$t_{ij}^{ab}(1) = \langle ab||ij\rangle / D_{ijab} \tag{8}$$

with energy

$$E_2 = \sum_{\substack{a>b \\ i>j}} \langle ab||ij\rangle t_{ij}^{ab}(1) \tag{9}$$

This is the second-order perturbation energy. The next iteration, also only of the linear terms, yields

$$\begin{aligned} t_{ij}^{ab}(2) = & \sum_{c>d} \langle ab||cd\rangle t_{ij}^{cd}(1) + \sum_{k>l} \langle kl||ij\rangle t_{kl}^{ab}(1) \\ & + \sum_{k,c} (-\langle kb||jc\rangle t_{ik}^{ac}(1) + \langle ka||jc\rangle t_{ik}^{bc}(1) \\ & + \langle kb||ic\rangle t_{jk}^{ac}(1) - \langle ka||ic\rangle t_{jk}^{bc}(1) \end{aligned} \tag{10}$$

and

$$E_3 = \sum_{\substack{a>b \\ i>j}} \langle ab||ij\rangle t_{ij}^{ab}(2) \tag{11}$$

The next iteration of the linear term would be the same as (1), except for using $t_{ij}^{ab}(2)$ in place of $t_{ij}^{ab}(1)$ to give $t_{ij}^{ab}(3;L)$. However, we show elsewhere[15] that this is not necessary since

$$E_4^D = \sum_{\substack{a>b \\ i>j}} \langle ab||ij\rangle t_{ij}^{ab}(3;L) = \sum_{\substack{a>b \\ i>j}} |t_{ij}^{ab}(2)|^2/D_{ijab} \tag{12}$$

The first nonlinear iteration yields

$$\begin{aligned} t_{ij}^{ab}(3;N) = \sum_{\substack{k>l \\ c>d}} & [\langle kl||cd\rangle\{t_{ij}^{cd}(1)t_{kl}^{ab}(1) - 2[t_{ij}^{ac}(1)t_{kl}^{bd}(1) \\ & + t_{ij}^{bc}(1)t_{kl}^{ac}(1)] - 2[t_{ik}^{ab}(1)t_{jl}^{cd}(1) + t_{ik}^{cd}(1)t_{jl}^{ab}(1)] \\ & + 4[t_{ik}^{ac}(1)t_{jl}^{bc}(1) + t_{ik}^{bd}(1)t_{jl}^{ac}(1)]\}] \end{aligned} \tag{13}$$

which provides the amplitudes for

$$E_4^Q = \sum_{\substack{a>b \\ i>j}} \langle ab||ij\rangle t_{ij}^{ab}(3;N) \tag{14}$$

The superscripts D and Q refer to the two components of fourth-order perturbation theory corresponding to double- and quadruple-excitation diagrams. This defines the perturbation-theory model DQ-MBPT(4). A similar consideration of the CCSD wavefunction, $\exp(T_1 + T_2)|\phi_0\rangle$, leads in addition to the fourth-order contribution of single excitations which we define as SDQ-MBPT(4). For the vast majority of cases the DQ-MBPT(4) energy differs from

CCD by less than 1 kcal/mol,[5] so (S)DQ-MBPT(4) is often nearly equivalent to CCD (CCSD); then it is not necessary to converge to the infinite-order solution of (5a). Another model used in this paper is D-MBPT(4), which is not as reliable as (S)DQ-MBPT(4).[14,16,28] Due to (12), though, it is very inexpensive and it generally benefits from some cancellation of errors. However, this model can be erroneous in difficult cases, so we always report a CCD result at critical points to guarantee that no unusual complications occur.

The triple excitations also contribute in fourth-order perturbation theory leading to a negative contribution that is at least as large as the individual SDQ contributions,[29] but since the triple excitations are an order of magnitude more time-consuming to compute than the SDQ components,[14,29] we hope that their net effect on most energy surfaces is unimportant. This will certainly not always be the case though. On the other hand, SDQ-MBPT(4) is simply a low-order iteration of the CCSD model that is usually close to the infinite-order value. Thus, this model would seems to be largely justified by including the two lowest categories of excitation operators just as in SD-CI. In both cases, selected terms are summed to all orders of perturbation theory instead of computing all terms of fourth order. Experience should eventually establish which procedure is better.

The main disadvantage of the MBPT/CCM approach, the restriction to a single reference function, is not essential to the theory but only to the current implementation (see References 30-32 for the multi-reference MBPT/CCM theory). To solve open-shell problems we normally use an unrestricted-Hartree-Fock (UHF) reference function. It is well-known that such functions can suffer from large amounts of spin contamination and are not suited to obtaining any surfaces except those that are the lowest of a given symmetry. However, the UHF function, unlike an RHF function, will usually allow a molecule to separate correctly into its fragments for all decomposition channels. In contrast, multi-reference-function techniques that include all configurations required to achieve correct separation would be intractable for even most three- and four-atom molecules. To limit the uncertainty introduced in using a UHF function for open shells, we monitor the multiplicity in the calculations. For some cases, such as the $\tilde{A}^1A''$ state of HNO in the present paper, it offers a caution on the interpretation of the results, while for other cases, such as the $^2A'$ HCO surface, no multiplicity problems are encountered.

For all the molecular states described in this study, the SCF reference function is given by a UHF wavefunction. The integrals over atomic functions were computed using Dunning's 4s3p[33] contraction of Huzinaga's 9s5p primitive basis set[34] for first-row atoms and Dunning's scaled (ζ=1.2) 3s contraction of Huzinaga's 4s primitive set for hydrogen. In the formyl radical study, a single set of d-type (Gaussian) polarization functions augments the atomic basis sets for carbon and oxygen, with exponents 0.75 and 0.85, respectively.[35] A set of p-type (Gaussian) polarization functions with exponent α=1.0 augments the hydrogen basis set.[35] For the HNO calculations, the exponents for the nitrogen and oxygen polarization functions are 0.92 and 1.02, respectively.[36]

For all molecules, molecular integrals were computed using the MOLECULE program.[37] Structure calculations for HCO and HNO were performed using the

GRNFNC and UMBPT programs.* The structural parameters and vibrational frequencies for the equilibrium structure and the hydrogen-dissociation transition state were predicted using GRADSCF codes.[38] A 6-31G** basis set was employed in these calculations.[39] The structural parameters for the triatomics have been optimized relative to D-MBPT(4) calculations.

In the following,the inexpensive D-MBPT(4) model is used for most points on the energy surface, while CCD and SDQ-MBPT(4) values are reported for barrier heights and dissociation energies. In the course of the discussion of the hydrogen dissociation reactions, we consider the barrier height and dissociation energy for each reaction. The electronic structure calculations predict values for the classical barrier height, E_b, and the classical dissociation energy, D_e. If vibrational zero-point energy corrections are included, we then refer to the critical energy, E_0, and the dissociation energy, D_0. The critical energy corresponds to the transition-state-theory activation energy at 0 K, while D_0 corresponds to the limit at 0K of the heat of reaction. It is also known as the conventional transition-state approximation to the vibrationally adiabatic ground-state barrier height or threshold energy.

III. GROUND STATE POTENTIAL ENERGY SURFACE FOR THE FORMYL RADICAL

A. Background

We have published the results of MBPT calculations for the formyl radical, HCO, including a description of the ground state potential energy surface.[3] Here we describe a more complete calculation of that surface.

Chemical reactions of the formyl radical are important in all combustion models that include formaldehyde; hence, all models for the oxidation of alkanes contain the reaction of the formyl radical. In addition to many bimolecular reactions of the radical, the unimolecular hydrogen decomposition reaction is important in many combustion models. Seery and Bowman,[40] McKellar and Norrish,[41] and Fifer[7] have all found the reaction HCO + M → H + CO + M to be important in analytical models that describe the oxidation of formaldehyde. The rate coefficient for the reaction has been estimated in various ways, but there is little agreement among the several papers.[7,42] A reasonable estimate of the rate coefficient for the reaction should be attainable if a reliable description of the potential energy surface is accomplished. In particular, an estimate of the critical energy and molecular information about the transition-state region are required.

There are several published theoretical studies of the formyl radical. Ab initio UHF calculations for the ground electronic state have been used to predict vibrational force constants[43] and to predict hyperfine coupling constants.[44] Nonempirical restricted Hartree-Fock (RHF) and CI calculations

---

* The program GRNFNC, written by G.D. Purvis, does SCF iterations and integral transformations. The program UMBPT, written by R.J. Bartlett and G.D. Purvis, does MBPT, CCD, and VP-DCI.

for the ground state and several low-lying excited states have been reported, along with SCF calculations of potential energy curves for hydrogen bending and hydrogen dissociation of the radical.[45] The first detailed correlated study of the ground-state potential energy surface was the study of the potential energy surfaces for several unimolecular reactions of HCO and COH.[46] The results of Dunning's calculations on the potential energy surface for hydrogen dissociation agree well with the perturbation theory results. Neither of the published correlated treatments, however, describe the angular variation of the least-energy pathway. Since this information is important for theoretical calculations of dynamical processes, we have extended our previous studies to include the angular dependence. For completeness, we also review the results of our dissociation-energy and molecular-structure predictions,[3] and we compare them with experimental and other theoretical values.

B. Potential Energy Surface for HCO + M → H + CO + M

There are few ways to test the accuracy of a potential energy surface calculation. Certainly an accurate calculation should yield accurate molecular structures of the reactants and the products. In addition, the predicted heat of reaction should agree well with the experimental value. If these tests are satisfied, then the hope that similar accuracy applies for predictions in the transition-state region may be justified.

In this study, equilibrium structural parameters were determined by minimizing the total electronic energy as a function of each of the degrees of freedom in the molecule. The total energy was calculated by adding the D-MBPT(4) estimate of the correlation energy to the energy calculated with the UHF wavefunction. The theoretically determined structural parameters for the formyl radical are compared with experimental values[47] in Table 1. The agreement between theory and experiment is excellent.

Table 1. Structural Parameters for Formyl Radical, HCO

	UHF	D-MBPT(4)	RHFCI[a]	Experiment[b]
R_{CH} (a_0)	2.078	2.10	2.116	2.126
R_{CO} (a_0)	2.218	2.245	2.249	2.220
θ_{HCO} (deg)	126.8	124	125.9	124.95

a. Reference 46.
b. Reference 47.

A more revealing test of the theory is the calculated values of the heat of reaction for the hydrogen dissociation. Recent experimental research on the dissociation process implies a dissociation energy equal to 15.5 kcal/mol.[48] The experimental value is compared with several different theoretical estimates in Table 2. It is apparent that each of the linked-diagram-related

theoretical methods and the CI calculation[46] give the dissociation energy with good accuracy. On the other hand, the UHF dissociation energy is more than 10 kcal/mol too low. In a series of calculations to determine the dissociation energies for the reactions

$$CH_iO \rightarrow CH_{i-1}O + H \qquad i = 1, 2, 3, \text{ or } 4$$

we have found that MBPT calculations of the quality described here give values that are 1 to 3 kcal/mol below published experimental values. Dissociation energy calculations at the SCF level, however, neither agree with experimental values nor reflect experimental trends. Thus it is necessary to include correlation energy effects if chemically accurate energy differences are desired.

Table 2. Empirical and Theoretical Values of Dissociation Energy for HCO

	$\Delta H_{R,300}$ (kcal/mol)
Experiment[a]	15.5 ± 1.5
Theoretical Values	
UHF	4.6
D-MBPT(4)	12.9
SDQ-MBPT(4)	12.9
CCD	13.0
SCF-CI[b]	12.2

a. Reference 48.
b. Reference 46.

The potential energy surface for the hydrogen-dissociation reaction of the formyl radical is computed at the D-MBPT(4) level. For 12 choices of the carbon-hydrogen bond length, the energy is minimized with respect to variations in the carbon-oxygen bond length and the bond angle. Only nonlinear geometries are considered. The nonlinear nuclear arrangements belong to the point group C_s, and the ground electronic state for HCO is X^2A'. This state correlates with the ground states of the products. The electronic energy at extrema on the surface are computed using higher energy levels of theory, SDQ-MBPT(4), and CCD. Some of the results are reported in Table 3 and the D-MBPT(4) results are displayed in Figure 1. The most striking result of the hypersurface calculation is the magnitude of the potential energy barrier at the transition state. A classical recombination barrier range of 6.7 kcal/mol (CCD) to 7.4 kcal/mol [D-MBPT(4)] is obtained from the various correlated calculations.

Table 3. Energy of HCO for Selected R_{CH} and Classical Barrier Height and Dissociation Energy at Several Levels of Calculation

			Energy + 113 E_h (E_h)[a]					
R_{CH} (a_0)	R_{CO}^{opt} (a_0)	θ_{HCO}^{opt}	UHF	D-MBPT(2)	D-MBPT(3)	D-MBPT(4)	SDQ-MBPT(4)	CCD
1.9	2.242	127.4	.27102	.6184	.6179	.6269	.6288	
2.1	2.245	124	.2769	.6259	.6248	.6343	.6363	.6288
2.4	2.21	122.5	.2689	.6175	.6166	.6264		
2.8	2.19	120	.2515	.598	.5961	.6065		
3.2	2.165	117.5	.24738	.5905	.5871	.5975		
3.35	2.15	115	.2488	.5904	.5871	.5973	.5998	.5922
4.0	2.13	112.5	.25625			.6017		
5.0	2.13	107	.2624	.6008	.5971	.6069		
∞ (20.0)	2.125	....	.2641	.6021	.5984	.6082	.6101	.6029
E_b (classical barrier)			.0281	.0355	.0377	.037	.0365	.0366
D_e (classical dissociation energy)			.0128	.0239	.0264	.0261	.0261	.0259

a. 1 E_h = 1 hartree = 627.5 kcal/mol

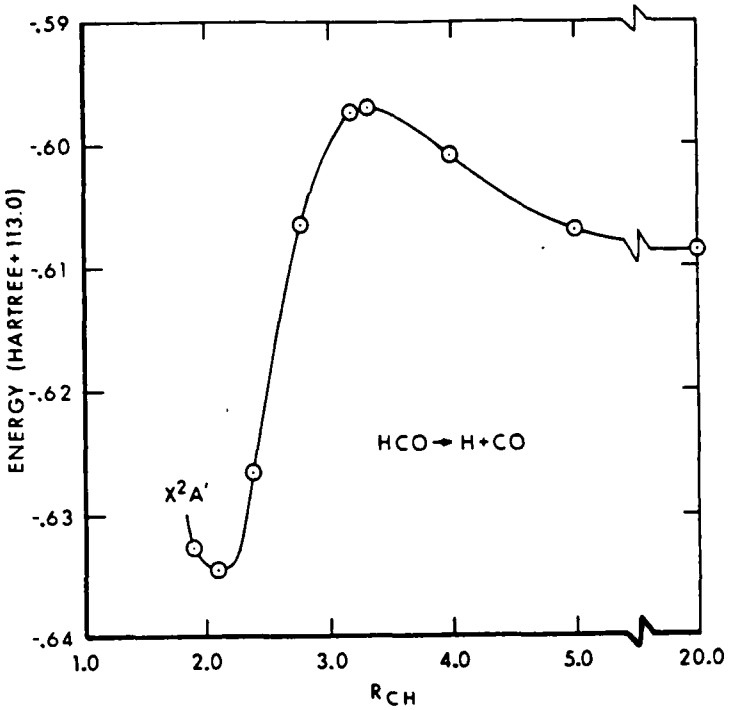

Figure 1. The Calculated [D-MBPT(4)] Potential Energy Curve for the Hydrogen Dissociation Reaction of the Formyl Radical
For each choice of R_{CH} shown, the bond angle and carbon-oxygen bond length were optimized.

These values should not be compared directly with the experimentally derived activation energy, 2 kcal/mol, in particular since the latter is a temperature-dependent quality. The experimental activation energy was determined for the temperature range, 298 K < T < 373 K, with H_2 as the third body.[49] The electronic energy difference between the barrier maximum and reactants, when corrected for the difference in zero-point vibrational energies, will be called the critical energy, E_0, for reaction. (See end of Section II.) Theoretical models that describe unimolecular reactions include an $\exp(-E_0/kT)$ factor, so that the critical energy accounts for a part of the observed chemical kinetic temperature dependence. To predict the critical energy, we must know the vibrational frequencies of the transition state species. Although theoreticians have demonstrated the capability to predict vibrational frequencies with good accuracy,[16,50] the effort expended to obtain very high accuracy encourages the use of simpler approaches. In this study, we predict vibrational frequencies using high-quality self-consistent-field calculations to predict the Cartesian force constants. The calculations are performed using the GRADSCF system of electronic structure codes. Although the basis sets used in computing the vibrational frequencies differed from those used in the MBPT calculations, the basis sets were of similar quality. Predicted frequencies for the equilibrium formyl radical and the saddle point are presented in Table 4. A comparison of the predicted and observed

frequencies[51-53] for the radical shows that this level of theory gives vibrational frequencies that exceed experiment by about 15%. On the other hand, our experience indicates that the zero-point vibrational energy differences are predicted with reasonable accuracy by the SCF calculations. Consequently, a good estimate of the critical energy for the hydrogen dissociation can be made. The results of the correlated calculations give an electronic energy barrier of approximately 23.1 kcal/mol, while the predicted zero-point energy change is -5.0 kcal/mol. Thus, the predicted critical energy for the dissociation reaction is about 18.1 kcal/mol.

The good accuracy obtained with the MBPT calculations in predicting the structural parameters of the formyl radical and the dissociation energy for the hydrogen dissociation reaction suggests that, in this instance, the use of a UHF wavefunction as the zero-order function does not introduce severe errors into the study of the potential energy surface. Furthermore, although the wavefunction was not a spin eigenfunction, the wavefunction did approximate the correct spin-multiplicity (2.0) at every point on the surface.[3] This result is not general, however, since only a single bond is being broken and the zero-order function is well-approximated by a single-determinant reference function.

Table 4. Vibrational Frequencies (cm^{-1}) for HCO and the Transition State for the Dissociation Reaction

Molecule	Predicted	Observed
ν_1 (CH stretch)	3050.7	2483[a]
ν_2 (CO stretch)	1932.2	1868.4[b]
ν_3 (HCO bend)	1247.7	1080.76[c]
Transition State		
ν_1 (reaction coordinate)	1216i	
ν_2 (CO stretch)	2187.0	
ν_3 (HCO bend)	557.4	

a. Reference 50.
b. Reference 51.
c. Reference 52.

IV. POTENTIAL ENERGY SURFACES FOR DISSOCIATION OF HYDROGEN NITROXIDE, HNO

A. Background

The chemistry and spectroscopy of hydrogen nitroxide, HNO, have been objects of experimental and theoretical study for many decades. The gas-phase recombination of hydrogen and nitrogen oxide represents a typical three-body reaction,

$$H + NO + M \rightarrow HNO + M \quad (R5)$$

However, three distinct bound electronic states of the product are accessible after recombination:

$$H(^2S) + NO(^2\Pi) + M \rightarrow HNO(X^1A') + M \quad (R6)$$

$$\rightarrow HNO(a^3A'') + M \quad (R7)$$

$$\rightarrow HNO(\tilde{A}^1A'') + M \quad (R8)$$

and formation of each of the product states has been proposed.[54-57] The reaction of hydrogen with nitric acid oxide produces a red emission corresponding to,[58-60]

$$HNO(\tilde{A}^1A'') \rightarrow HNO(X^1A') + h\nu \quad (R9)$$

The branching ratios for the three recombination reactions are unknown, and the mechanism for production of the A^1A'' state of HNO is not established. Clyne and Thrush[51] have proposed that A^1A'' state is not produced directly, but that recombination occurs to the a^3A'' state followed by a radiationless transition

$$HNO(a^3A'') \rightarrow HNO(\tilde{A}^1A'') \quad (R10)$$

This mechanism has been disputed,[61] primarily because Clyne and Thompson assumed that no recombination barrier occurred on the a^3A'' surface. A more recent theoretical study of the potential energy curves for the molecule demonstrates the existence of potential barriers for both the a^3A'' and $\tilde{A}^1A''$ surfaces, but the predicted barriers are low enough, 3.7 kcal/mol and 7.8 kcal/mol, for hydrogen recombination to occur thermally.[62] These CI calculations of the potential energy surfaces, however, used SCF energy-optimized structures of the ground electronic state for all three of the low-lying curves. In this study, we compute potential energy curves for the X^1A', a^3A'', and $\tilde{A}^1A''$ states, optimizing R_{NO} and θ for each value of R_{NH} computed on each of the curves.

The energy separation of the X^1A' and $\tilde{A}^1A''$ states has been determined by a number of experiments to lie in the neighborhood of 1.63 eV.[59,60,63,64] Recent experiments on the $O_2(^1\Delta_g)$-sensitized chemiluminescence of HNO suggest the existence of a triplet state about 0.8 eV above the ground state.[65] A more recent experiment established the excitation energy to be 0.85 eV (19.6 kcal/mol).[66] Several theoretical studies predict excitation energies

for these two transitions that agree moderately well with the experimental values.[62,67,68] Since we wish to estimate relative rates of recombination into the three states, it is important that our predicted potential energy curves accurately predict the structure of HNO in each state and the energy separating the states. Therefore, we report D-MBPT(4) energy-optimized structures for the X^1A', a^3A'', and $\tilde{A}^1A''$ states of HNO, as well as MBPT/CCM values for the excitation energies corresponding to the $X^1A' \rightarrow a^3A''$ and $X^1A' \rightarrow \tilde{A}^1A''$ processes. Subsequent sections describe the theoretically determined dissociation energies for each of the bound states and enumerate the details of the potential energy surfaces. Finally, we estimate the low-pressure recombination rate ratios.

B. Predicted Structures

The structures of HNO in the ground and $\tilde{A}^1A''$ excited states were established by Dalby in his classic study.[63] A comparison between the experimental structural parameters[63,69] and those obtained from D-MBPT(4) calculations is offered in Table 5. Excellent agreement between theory and experiment is found for each state, although the predicted parameters for the ground state agree more closely with Dalby's values than do those for the excited state. No empirically derived structural parameters are available for the a^3A'' state. The predicted parameters obtained in our study differ signficantly from those predicted in various SCF studies. An SCF calculation using a 4-31G basis set predicts an NO bond length of 2.382 a_0, an NH bond length of 1.911 a_0, and a bond angle of 114.8°.[66] This structure agrees better with the structural parameters for the A^1A'' state than with those of the triplet state. An SCF calculation using the extended 6-31G** basis set predicts an NO bond length of 2.322 a_0, and an NH bond length of 1.915 a_0, both in reasonable agreement with the D-MBPT(4) results. However, in this case the SCF predicted bond angle, 112.1°, differs by more than 11° from the MBPT predicted value. Interestingly, SCF calculations for the X^1A'' state predict the bond angles well, 108.9°, but do poorly at predicting the bond lengths (R_{NO}, 2.22 a_0, R_{NH}, 1.95 a_0).[70] Since the MBPT calculations predict structural parameters that agree well with experiment for the two singlet states, we contend that the structural parameters predicted by the MBPT calculations for the a^3A'' are preferable to those predicted by the SCF-level calculation. It should be noted that each of the triplet state wavefunctions had a multiplicity close to 3.0. In particular, the multiplicity for the 4-31G calculation is 3.02, that for the 6-31G* calculation is 3.02, and the result for the D-MBPT(4) calculation is 3.01.

C. Excitation Energies

In addition to establishing the structures for HNO in the X^1A' and $\tilde{A}^1A''$ electronic states, Dalby determined that the excitation energy corresponding to the process $X^1A' \rightarrow \tilde{A}^1A''$ is 1.63 eV.[63] Recently, Ishiwata, et al., reported that the excitation energy for the process $X^1A' \rightarrow a^3A''$ equals 0.85 eV.[66] We summarize in Table 6 the computed electronic energies for the X^1A', a^3A'', and $\tilde{A}^1A''$ states of HNO. Note that the UHF calculations predict that the ground state is a triplet state. Each of the correlated calculations, on the other hand, orders the electronic states correctly.

To compare predicted excitation energies with experimental values for adiabatic excitations, the zero-point energy for each of the states must be

Table 5. Comparison of Predicted and Experimental Structural Parameters for HNO and NO

	D-MBPT(4)	Experiment	Reference
HNO			
X^1A'			
R_{NO} (a_0)	2.307	2.290	63
R_{NH} (a_0)	2.007	2.009	
θ (deg)	107.8	108.6	
a^3A''			
R_{NO} (a_0)	2.302	.....	
R_{NH} (a_0)	1.938	.....	
θ (deg)	123.8	.....	
$\tilde{A}^1A''$			
R_{NO} (a_0)	2.31	2.345	63
R_{NH} (a_0)	1.94	1.985	
θ (deg)	114.4	116.3	
NO			
$X^2\Pi$			
R_{NO} (a_0)	2.149	2.1747	69

included. Experimental frequencies are available for the X^1A' and $\tilde{A}^1A''$ states, but no experimental data are available for the a^3A'' state. Therefore we have computed vibrational frequencies for the X^1A' and a^3A'' states in order to compute the zero-point energy difference for the $X \rightarrow a$ transition. As may be seen in the comparison shown in Table 7, there is poor agreement between the experimentally determined frequencies and those predicted by the SCF calculations. If, however, the frequencies for each state are reduced by 15%, the ground state frequencies agree reasonably well with the experimental values. As noted during our discussion of the formyl radical, however, the SCF calculations generally yield zero-order energy differences that agree well with experiment, so we use the SCF prediction for the zero-point energy change, 1.3 kcal/mol.

The theoretically calculated and experimental excitation energies are compared in Table 8. We report MBPT and CCD calculations for excitations to

Table 6. Electronic Energy Predictions for Equilibrium Structures of HNO

Theoretical Method	X^1A' (E_h)	a^3A'' (E_h)	$\tilde{A}^1A''$ (E_h)	$X^1A' \rightarrow a^3A''$ (kcal/mol)	$X^1A' \rightarrow \tilde{A}^1A''$ (kcal/mol)
D-MBPT(2)	-130.2314	-130.19730	-130.1656	21.4	41.3
D-MBPT(3)	.2302	.2031	.1779	17.0	32.8
D-MBPT(4)	.2424	.2110	.1853	19.7	35.8
D-MBPT(6)	.2459	.2131	.1883	20.6	35.9
SD-MBPT(4)	.2488	.2176	.1925	19.6	35.3
DQ-MBPT(4)	.2346	.2053	.1802	18.4	34.1
SDQ-MBPT(4)	.2410	.2119	.1875	18.3	33.6
CCD	.2340	.2049	.1804	18.3	33.6

the a^3A'' and $\tilde{A}^1A''$ states. These predictions may be compared to experimental excitation energies and those obtained via configurations interaction calculations.[56,62] The MBPT and CCD results include zero-point energy corrections. The linked-diagram related calculations yield excitation energies that are lower than the experimental values. These results are similar to the CI results of Wu, et al.[56] That our calculations predict the excitation energy to the $\tilde{A}^1A''$ state to be too low is not surprising, since the UHF wavefunction for that state has a computed spin multiplicity of about 2.24. Obviously the wavefunction contains a substantial amount of triplet state character, leading to a low value for the excitation energy. The excitation energy for a^3A'' state agrees well with experiment. The detailed analysis of the contributions to the correlation energy, Table 6, shows that the second-order, double-excitation contribution recovers almost all the error contained in the UHF calculation. Furthermore, even though the fourth-order MBPT calculation is not completely converged (the calculation is said to be converged if the contribution to the correlation energy, at order n say, is less that 10^{-4}), the relative energies determined at that level of calculation agree well with the D-MBPT(6) and converged CCD results. Finally, the agreement between each of the fourth-order MBPT calculations that include both double- and quadruple-excitation diagrams, DQ-MBPT(4) and SDQ-MBPT(4), and the CCD calculations suggest that the difference between CCD and D-MBPT(4) is due to the inclusion of quadruple-excitation effects in the CCD calculations.

Table 7. Vibrational Frequencies of HNO

State, Mode	~~Predicted~~[a]	Experiment
X^1A'		
NH Stretch	3297	2684.7[b]
NO Stretch	1971	1500.8[c]
HNO Bend	1718	1565.3[c]
a^3A''		
NH Stretch	3590	.....
NO Stretch	1511	.....
HNO (Bend)	966	.....

a. SCF calculation using GRADSCF (Reference 38). Basis set: 6-31G** (Reference 39).
b. Reference 71.
c. Reference 72.

Table 8. Adiabatic Excitation Energies (kcal/mol) for HNO

	D-MBPT(4)	D-MBPT(6)	DQ-MBPT(4)	SDQ-MBPT(4)	CCD	Exp.	CI[a]	CI[b]
$X^1A' \rightarrow a^3A''$	18.4	19.2	17.0	16.9	16.6	19.7[c]	16.3	21.4
$X^1A' \rightarrow \tilde{A}^1A''$	35.1	36.1	33.5	32.7	32.9	37.6[d]	36.9	43.8

a. Reference 56.
b. Reference 62.
c. Reference 66.
d. Reference 63.

Since the MBPT calculations predict the energy separations of the three-lowest electronic states of HNO with good accuracy, we now turn to the representation of the potential energy surfaces for each of these states.

D. Potential Energy Curves for Hydrogen Dissociation Reactions of HNO

The results presented in the previous sections demonstrate that the MBPT calculations predict equilibrium structures for HNO with excellent accuracy and the relative energies of the three states with good accuracy. To represent a potential energy surface accurately, however, requires that the theoretical method predict the dissociation energy with good accuracy also. The dissociation energy, D_0, of HNO in the ground electronic state, 48.6 kcal/mol,[54] is well known and the dissociation energies from the two lowest excited states can be deduced since the excitation energies are known and since all three states dissociate to the same products, $H(^2S) + NO(^2\Pi)$. Thus, the dissociation energy for the a^3A'' state is 29.1 kcal/mol, while that for the $\tilde{A}^1A''$ state is 11.0 kcal/mol.

To compare the theoretical and experimental dissociation energies, the theoretically determined electronic energies must be corrected for vibrational zero-point energy changes. Using experimental frequencies for the X^1A' state of HNO and the ground $^2\Pi$ state of NO, the zero-point energy change for the dissociation of ground state nitrosyl hydride is -5.56 kcal/mol. Combining this result with the estimated frequencies for the a^3A'' and the experimental data for the $\tilde{A}^1A''$ state, the zero-point energy changes for dissociation from those states are 4.4 and 4.8 kcal/mol, respectively. Listed in Table 9 are predicted values for the hydrogen dissociation energies of the three lowest electronic states of nitrosyl hydride. The most obvious result of the calculations is the inadequacy of the self-consistent-field method for predicting relative energies. The encouraging result of the study is that each of the MBPT and CCD calculations gives good results for each of the dissociation energies. It is particularly encouraging that the D-MBPT(4) calculations predict the dissociation energies well since this is the level of theory that is least expensive for calculating the hypersurfaces for each reaction.

Table 9. Dissociation Energies for HNO

State	D_0 (kcal/mol)						
	E_{zp}	UHF	D-MBPT(4)	DQ-MBPT(4)	SDQ-MBPT(4)	CCD	Exp.[a]
X^1A'	-5.6	19.3	46.2	45.2	44.6	46.1	48.6
a^3A''	-4.2	23.8	27.9	28.2	27.6	29.1	29.1
A^1A''	-4.8	14.2	11.1	11.4	11.7	13.1	11.0

a. Reference 63.

The results of D-MBPT(4) calculations for the potential energy surfaces corresponding to each of the dissociation reactions are summarized in Table 10. For each value of the NH bond length, the electronic energy predicted by D-MBPT(4) calculations is minimized as a function of the NO bond length and the HNO angle. These parameters are presented in Table 10 for each of the three electronic states. In addition, we provide the results of both the UHF and D-MBPT(4) electronic structure calculations. The most obvious difference between the correlated and uncorrelated results are the classical dissociation energy and classical barrier estimates for the ground electronic state. In that case, UHF calculations predict a dissociation barrier about 4 kcal/mol greater than D_e for this electronic state, whereas the D-MBPT(4) calculations predict a negligible difference. The interesting and important results of this work are the estimates of classical recombination barriers for each of the electronic states. The D-MBPT(4) calculations predict almost no barrier for recombination into the ground electronic state, a barrier equal to 7.1 kcal/mol for formation of HNO in the a^3A'' state and a barrier equal to 14.0 kcal/mol for formation of HNO in the $\tilde{A}^1A''$ state. The recombination barriers significantly exceed those determined using configuration interaction calculations.[62] The CI calculations, however, were constrained by a small basis set and the use of structures optimized for the ground electronic state at each value of R_{NH}, so the differences between those results and the results presented here are not shocking. The UHF calculations predict recombination barriers for the two excited states that differ only by 1.8 kcal/mol. However, it should be noted that our UHF barrier calculations do not correspond to transition state structures optimized at the SCF level.

Another interesting aspect of the calculated potential surfaces is the variation in the angular dependence for each of the states. Both of the singlet states demonstrate a marked increase in the HNO bond angle as the hydrogen moves away from the NO fragment, while the triplet state shows very little angular variation of the optimal structure for any choice of R_{NH}. In fact, the variation of the electronic energy as a function of the bond angle in the triplet state is so slight that the variation in bond angle shown in Table 10 is probably due to the coarseness of the grid used to optimize the

Table 10. Electronic Energy Predictions for HNO at Selected Values of R_{NH} for Each State and Classical Dissociation Energy and Barrier Height for Each State

X^1A'					a^3A''					A^1A''				
R_{NH}	R_{NO}	θ	UHF[a]	D-MBPT(4)[b]	R_{NH}	R_{NO}	θ	UHF[a]	D-MBPT(4)[b]	R_{NH}	R_{NO}	θ	UHF[a]	D-MBPT(4)[a]
1.9	2.32	107.8	.8167	.2409	1.85	2.28	125.3	.8222	.2096	1.9	2.288	114	.8083	.1846
2.007[c]	2.307	107.8	.8172	.2424	1.938[c]	2.302	123.8	.8230	.2110	1.94[c]	2.31	114.4	.8078	.1853
2.5	2.142	111.0	.7896	.2129	2.5	2.283	121.0	.7831	.1770	2.6	2.22	116.7	.7686	.1490
3.0	2.147	111.2	.7708	.1680	3.2[d]	2.168	122.1	.7637	.1485	3.01[d]	2.18	117.8	.7606	.1377
3.5	2.148	112.0	.7713	.1597	4.0	2.182	124.5	.7697	.1571	4.0	2.14	126.5	.7708	.1523
4.0	2.148	114.0	.7739	.1590										
20.0	2.149	...	.7775	.1599	20.0	2.149	...	.7775	.1599	20.0	2.149	...	.7775	.1599
D_e[e]			24.9	51.8				28.0	31.2				19.0	15.9
E_b[e]			(29.1)[f]	52.3				(36.7)[f]	38.3				(29.5)[f]	29.9

a. Energy + 129.0 E_h.
b. Energy + 130.0 E_h.
c. Predicted structural parameters of equilibrium configuration.
d. Predicted structural parameters of transition state.
e. Units: kcal/mol
f. UHF energy barrier does not correspond to UHF optimized transition state structure.

angle. The difference in the bond angle variation in the three states, however, serves to emphasize the differences in relative energies that would be obtained were one to use SCF-optimized structures of the ground state for correlation calculations in all three states.

The potential energy as a function of dissociation coordinate is shown for the three electronic states in Figure 2. An interesting feature of the curves is the broadness of the barrier in the transition state region of the two excited states. This feature suggests that quantum mechanical tunneling through these barriers should be slow. Hence, it seems unlikely that tunneling is a reasonable explanation for the observed diffuseness in the excitation spectra. In fact, our results support Freedman's suggestion that the break off in the rotational structure corresponds to an intersystem crossing to an electronic state with an accessible continuum.[57] In the next section we consider possible mechanisms for the formation of HNO in the $\tilde{A}^1A''$ state, the origin of the observed chemiluminescence.

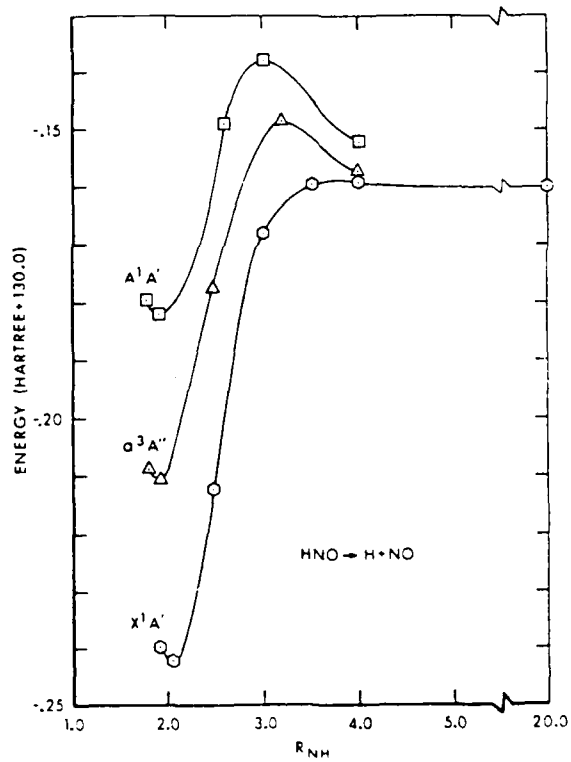

Figure 2. The Calculated [D-MBPT(4)] Potential Energy Curves for the Three Lowest Electronic States of Nitrosyl Hydride
For each choice of R_{NH} shown, the bond angle and nitrogen-oxygen bond length were optimized for each of the states.

E. Relative Rates for Recombination Into Three Electronic States of HNO

In order to obtain estimates of the relative rates for the recombination of hydrogen and nitrogen oxide to form HNO in each of the three electronic states, we use a simplified theory of unimolecular reactions developed by Troe and coworkers.[73-75] In his review paper on the predictive possibilities of unimolecular rate theory, Troe cites the lack of detailed knowledge of the potential energy hypersurfaces and of the intermolecular energy transfer processes. We have described the details of the potential energy surfaces for three states of nitrosyl hydride, so we have supplied one of Troe's unknowns. The details of the energy transfer processes stand outside the range of this study, but by invoking the strong collision postulate, relative recombination rates for the formation of nitrosyl hydride may be obtained.

Troe[75] expresses the limiting low pressure, pseudo-first-order rate coefficients, k_0, for thermal dissociations as

$$k_0 = \beta_c k_0^{sc} \tag{15}$$

where β_c represents the temperature dependent collision efficiency and k_0^{sc} represents the strong-collision form of the limiting rate coefficient. The corresponding rate coefficient for recombination $k_{rec,0}$, is obtained from k_0 with the equilibrium constant K_c, via

$$k_{rec,0} = k_0 K_c^{-1} \tag{16}$$

Troe gives an expression for k_0^{sc} in terms of factors such as the harmonic density of states, the Lennard-Jones collision frequency, the vibrational partition function, and the critical energy, E_0, as well as terms to account for anharmonicity corrections, the energy dependence of the density of states, and rotational effects. We use Eq. (1) of Reference 75 to estimate k_0^{sc}. Expressions to evaluate each of the factors in that equation are summarized in Reference 74. For the purpose of this discussion, β_c=1 for the unimolecular dissociation reaction of each state of HNO.

One can predict the rate coefficients for unimolecular dissociation of HNO in each of the three states, provided that molecular data describing the reacting system are available. The data required are the molecular structure and vibrational frequencies for the reactant and the activated complex, as well as the energy barrier to be overcome during the reaction, the critical energy. All of these data are available, in principle, from the results of the potential energy surface calculations. However, as was discussed in the preceding section, the theoretically estimated values for the vibrational frequencies agree poorly with experimentally determined values. Consequently, the rate coefficient calculations described here use empirical frequencies for the X^1A' and A^1A'' states, and estimated frequencies for the a^3A'' state and the activated complexes. The estimated frequencies are chosen to agree with the zero-point vibrational energy differences predicted by GRADSCF[39] calculations.

In order to estimate relative recombination rates, we must also determine the ratios of the equilibrium constants for the different electronic states. These ratios can be obtained using the molecular data predicted by the MBPT calculations, along with the predicted excitation energies. Because the masses of all the chemical species are the same in the three dissociation

reactions, no effect of translational degrees of freedom will appear when the equilibrium coefficient ratio is taken.

For the X^1A' and a^3A'' states, we have

$$\frac{K_c(a^3A'')}{K_c(X^1A')} = \frac{(q_{el}q_{vib}q_{rot})a^3A''}{(q_{el}q_{vib}q_{rot})X^1A'} \tag{17}$$

Since the products of dissociation of HNO from each of these states are identical, it is easy to show that

$$\frac{(q_{el})a^3A''}{(q_{el})X^1A'} = 3 \exp\,[\Delta E(X^1A' \rightarrow a^3A'')/kT] \tag{18}$$

where $\Delta E(X^1A' \rightarrow a^3A'')$ is the excitation energy, and the factor 3 accounts for the degeneracy of the triplet state. The vibrational and rotational partition function ratios are obtained by standard statistical mechanical methods. A completely similar treatment allows the determination of the equilibrium constant ratio for the X^1A' and $\tilde{A}^1A''$ states.

We list in Table 11 the molecular parameters needed to estimate k_0 for dissociation from each of the three electronic states, and to estimate the equilibrium constant ratios. In Table 12, we summarize the predicted k_0's and K_c ratios for a T = 300 K. The recombination ratios for the two excited states relative to the ground state are given by

$$\frac{k_{rec}(X^1A')}{k_{rec}(a^3A'')} = \frac{k_0(X^1A')}{k_0(a^3A'')} \cdot \frac{K_c(a^3A'')}{K_c(X^1A')} \tag{19}$$

and

$$\frac{k_{rec}(X^1A')}{k_{rec}(\tilde{A}^1A'')} = \frac{k_0(X^1A')}{k_0(\tilde{A}^1A'')} \cdot \frac{K_c(\tilde{A}^1A'')}{K_c(X^1A')} \tag{20}$$

For T = 300 K, we obtain

$$\frac{k_{rec}(X^1A')}{k_{rec}(a^3A'')} \simeq 1.8 \times 10^5$$

and

$$\frac{k_{rec}(X^1A')}{k_{rec}(\tilde{A}^1A'')} \simeq 1.77 \times 10^{10}$$

Table 11. Molecular Data for Hydrogen Nitroxide (cm^{-1}, amu $Å^2$, kcal/mol)

State/Property	ν_1	ν_2	ν_3	I_a	I_b	I_c	Adiabatic Excitation Energy[a]
X^1A'	2719	1505	1564	13.060	12.15	0.91	...
a^2A''	2990	1111	771	13.22	12.61	0.62	18.4
(a^3A'')[b]	...	1320	150	15.28	13.24	2.05	...
$\tilde{A}^1A''$	2854	981	1421	13.12	12.35	0.76	35.1
$(\tilde{A}^1A'')$[b]	...	1640	250	13.64	12.06	1.58	...

a. D-MBPT(4) prediction.

b. Data for saddle point in hydrogen dissociation reaction channel. There is not saddle point on the X^1A' surface.

Table 12. Low Pressure Rate Coefficients and Equilibrium Constant Ratios for HNO, T = 300 K

State	k_0 (cc mol^{-1} s^{-1})	K_c ratio
X^1A'	1.43×10^{17}	...
a^3A''	8.09×10^{-9}	6.65×10^{13}
$\tilde{A}^1A'$	3.04×10^{-3}	3.5×10^{25}

These predictions suggest that direct recombination into the excited singlet state, $\tilde{A}^1A''$, is an unlikely source for the chemiluminescence observed in the recombination of hydrogen and NO. The results do not exclude the excited triplet state, a^3A'', as an intermediate state in the chemiluminescene, via the mechanism

$$H(^2S) + NO(^2\Pi) \rightarrow HNO(a^3A'')$$

$$HNO(a^3A'') \rightarrow HNO(\tilde{A}^1A'')$$

However, the estimate of the number of molecules formed in the triplet state is low enough that these results cannot be interpreted as substantiating this two-step mechanism. Perhaps the best mechanism to propose for populating the $\tilde{A}^1A''$ state is the reverse of the process responsible for the break-off in rotational structure observed for the same state. Thus, intersystem crossing between the continuum states associated with the X^1A' state may be cited.

V. DISCUSSION

The results presented here provide a substantial test of the ability of MBPT to provide chemically useful information about potential energy surfaces. Although the limitations imposed by the restriction to a single determinant reference function limit the applicability of the method and give caution to some of the numerical results, use of UHF reference functions does not appear to prevent the theorist from obtaining chemically useful results. As noted in our previous work on HCO,[3] although the UHF reference function for the ground electronic state was not a pure doublet state, the spin multiplicity changed very little as a function of the position on the hypersurface. In the examples discussed here, the reference function for the $\tilde{A}^1A''$ state of HNO suffered from large amounts of spin contamination. The spin-multiplicity of the wavefunction of equilibrium configuration is 2.26, rather than 1.0, and it is this spin contamination that causes the relatively large error in the computed [SDQ-MBPT(4)] excitation energy, 4.7 kcal/mol. On the other hand, the spin multiplicity of the wavefunction at the saddle point on the $\tilde{A}^1A''$ surface is 2.36. Clearly, the spin does not vary strongly as a function of position on the surface, leaving the hope that relative energies on the surface are determined with good accuracy. In support of this point, one notes that dissociation energy predictions for the $\tilde{A}^1A''$ state agree more closely with the value derived from experimental data than the excitation energy predictions agree with that experimental datum. It is the case,

however, that the calculations for the X^2A' state of HCO and the X^1A' and a^3A'' states of HNO avoid the spin multiplicity problems encountered in the calculations for the $\tilde{A}^1A''$ state of HNO. Consequently, we are less cautious in our conclusions concerning those electronic states.

The results reported here also demonstrate the necessity of including correlation energy effects when studying potential energy surfaces. In the case of HNO, SCF calculations misorder the electronic states and yield poor results for the dissociation energy of each state. In addition, the SCF results predict a barrier to recombination on the X^1A' surface. Self-consistent-field calculations for HCO yield a poor prediction for the dissociation energy of that radical, whereas each of the correlation calculations that include correlation gives a value that agrees well with the experimental result.

ACKNOWLEDGMENT

This research was aided by collaboration with Drs. Rodney Bartlett and George Purvis. Their research efforts were sponsored, in part, by the Air Force Office of Scientific Research by a contract to Battelle Memorial Institute. We acknowledge the fine cooperation by the staff of the Ballistic Research Laboratory's Computational Support Group.

REFERENCES

1. **Eyring, H., and Polanyi, M., "Uber Einfache Gasreaktionen,"** Z. Phys Chem., Vol. B12, p. 279, 1931.

2. **Bauschlicher, Jr., C.W., Haber, K., Schaefer, III, H.F., and Bender, C.F.,** "Concerted Non-Least-Motion-Pathway for the Singlet Methylene Insertion Reaction $CH_2(^1A_1) + H_2 \rightarrow CH_4$," J. Amer. Chem. Soc., Vol. 99, p. 3610, 1977.

3. **Adams, G.F., Bent, G.D., Purvis, G.D., and Bartlett, R.J., "The Electronic** Structure of the Formyl Radical, HCO," J. Chem. Phys., Vol. 71, p. 3697, 1979.

4. **Harding, L.B., and Pople, J.A., "A Moller-Plesset Study of the H_4CO** Potential Energy Surface," Potential Energy Surfaces and Dynamics Calculations, D.G. Truhlar, ed., Plenum, NY, 1981.

5. **Bartlett, R.J., and Pruvis, G.D., "Molecular Applications of Coupled Cluster** and Many-Body Perturbation Methods," Physica Scripta, Vol. 21, p. 255, 1980.

6. **Bent, G.D., Adams, G.F., Bartlett, R.J., and Purvis, G.D., "Many-Body** Perturbation Theory Electronic Structure Calculations for the Methoxy Radical. I. Determination of Jahn-Teller Energy Surfaces, Spin-Orbit Splitting, and Zeeman Effect," J. Chem. Phys., Vol. 76, p. 4144, 1982.

7. **Fifer, R.A., and Holmes, H.E., "High Temperature Pyrolysis of Methyl and** Ethyl Nitrate", Proceedings of the 17th Symposium (International) of the Combustion Institute, Combustion Institute, Pittsburgh, PA, 1979.

8. **Brueckner, K.A., and Levinson, C.A., "Approximate Reduction of the Many-Body** Problem for Strongly Interacting Particles to a Problem of Self-Consistent Fields," Phys. Rev., Vol. 97, p. 1344, 1955; K.A. Brueckner, "Two-Body Forces and Nuclear Saturation. III. Details of the Structure of the Nucleus," Phys. Rev., Vol. 97, p. 1353, 1955; K.A. Brueckner, R.J. Eden, and N.C. Francis, "High-Energy Reactions and the Evidence for Correlations in the Nuclear Ground-State Wavefunction," Phys. Rev., Vol. 98, p. 1445, 1955; K.A. Brueckner, "Many-Body Problems for Strongly Interacting Particles. II. Linked Cluster Expansion," Phys. Rev., Vol. 100, p. 36, 1955.

9. **Goldstone, J., "Derivation of the Brueckner Many-Body Theory,"** Proc. Roy. Soc. Lond., Ser. A, Vol. 239, p. 267, 1957.

10. **Kelly, H.P., "Applications of Many-Body Diagram Techniques in Atomic** Physics," Advan. Chem. Phys., Vol. 14, p. 129, 1969.

11. **Kummel, H. "Compound Pair States in Imperfect Fermi Gases,"** Nucl. Phys., Vol. 22, p. 177, 1969.

12. **Cizek, J., "On the Use of the Cluster Expansion and the Technique of** Diagrams in Calculations of Correlation Effects in Atoms and Molecules," Advan. Chem. Phys., Vol. 14, p. 33, 1969; J. Cizek. J.J. Paldus, and L. Stroubkova, "Cluster Expansion Analysis for Delocalized Systems," Int. J. Quantum Chem., Vol. 3, p. 149, 1969.

13. **Paldus, J.J., and Cizek, J., "Relation of Coupled Pair Theory, CI, and Some** Other Many-Body Approaches, Energy, Structure, and Reactivity, D.W. Smith and W.B. McCrae, eds., Wiley, New York, p. 389, 1973.

14. **Bartlett, R.J., and Purvis, G.D., "Many-Body Perturbation Theory, Coupled-**Pair Many-Electron Theory, and the Importance of Quadruple Excitations for the Correlation Problem," Int. J. Quantum Chem., Vol. 14, p. 561, 1978.

15. **Bartlett, R.J., and Shavitt, I., "Comparison of High-Order Many-Body** Perturbation Theory and Configuration Interaction for H_2O," Chem. Phys. Lett., Vol. 50, p. 120, 1978.

16. **Bartlett, R.J., Shavitt, I., and Purvis, G.D., "The Quartic Force Field of** H_2O Determined by Many-Body Methods that Include Quadruple Excitation Effects," J. Chem. Phys., Vol. 71, p. 781, 1979.

17. **Redmon, L.T., Purvis, G.D., and Bartlett, R.J., "Accurate Binding Energies** of Diborane, Borane Carbonyl, and Borazane as Determined by Many-Body Perturbation Theory," J. Amer. Chem. Soc., Vol. 101, p. 2856, 1979.

18. **Redmon, L.T., Purvis, G.D., and Bartlett, R.J., "The Unimolecular** Isomerization of Methyl Isocyanide to Methyl Cyanide (Acetonitrile)," J. Chem. Phys., Vol. 69, p. 5386, 1978.

19. **Redmon, L.T., Purvis, G.D., and Bartlett, R.J., "Correlation Effects in the** Isomeric Cyanides: HNC→HCN, LiNC→LiCN, and BNC→BCN," J. Chem. Phys., Vol. 72, p. 986, 1980.

20. **Pople, J.A., Seeger, R., and Krishnan, R., "Variational Configuration** Interaction Methods and Comparison with Perturbation Theory," Int. J. Quantum Chem. Symp., Vol. 11, p. 149, 1977.

21. **Pople, J.A., Krishnan, R., Schlegel, H.B., and Binkley, J.S., "Electron** Correlation Theories and Their Application to the Study of Simple Reaction Potential Surfaces," Int. J. Quantum Chem., Vol. 14, p. 545, 1978.

22. **Robb, M.A., "Application of Many-Body Perturbation Methods in a Discrete** Orbital Basis Set," Chem. Phys. Lett., Vol. 20, p. 274, 1973.

23. **Sinanoglu, O., "Many-Electron Theory of Atoms, Molecules, and Their** Interactions," Advan. Chem. Phys., Vol. 6, p. 315, 1964.

24. **Freemen, D.I., and Karplus, M., "Many-Body Perturbation Theory Applied to** Molecules: Analysis and Correlation Energy Calculation for Li_2, N_2, and H_2," J. Chem. Phys., Vol. 64, p. 2641, 1976.

25. Harris, F.E., "Coupled Cluster Methods for Excitation Energies," Int. J. Quantum Chem. Symp., Vol. 11, p. 403, 1977.

26. Bartlett, R.J., and Purvis, G.D., "Electron Correlation in Large Molecules with Many-Body Methods," Ann. NY Acad. Sci., 1980.

27. Walch, S.P., Dunning, Jr., T.H., Raffinetti, R.C., and Bobrowicz, F.W., "A Theoretical Study of the Potential Energy Surface for $O(^3P) + H_2$," J. Chem. Phys., Vol. 72, p. 406, 1980.

28. Purvis, G.D., and Bartlett, R.J., "The Potential Energy Curve for the $X1\Sigma_g^+$ State of Mg_2 Calculated with Coupled-Pair Many-Electron Theory," J. Chem. Phys., Vol. 71, p. 549, 1979.

29. Krishnan, R., Frisch, M.J., and Pople, J.A., "Contribution of Triple Substitutions to the Electron Correlation Energy in Fourth-Order Perturbation Theory," J. Chem. Phys., Vol. 72, p. 4244, 1980.

30. Brandow, B.H., "Linked Cluster Expansions for the Nuclear Many-Body Problem," Rev. Mod. Phys., Vol. 39, p. 771, 1967.

31. Lindgren, I., "A Coupled-Cluster Approach to the Many-Body Perturbuation Theory for Open-Shell Systems," Int. J. Quantum Chem. Symp., Vol. 12, p. 33, 1978.

32. Hose, G., and Kaldor, V., "A General-Model-Space Diagrammatic Perturbation Theory," Physica Scripta, Vol. 21, p. 357, 1980.

33. Dunning, Jr., T.H., "Gaussian Basis Functions for Use in Molecular Calculations. I. Contraction of (9s5p) Atomic Basis Sets for the First-Row Atoms," J. Chem. Phys., Vol. 53, p. 2823, 1970.

34. Huzinaga, S., "Gaussian-Type Functions for Polyatomic Systems." I., J. Chem. Phys., Vol. 42, p. 1293, 1965.

35. Dunning, Jr., T.H., and Hay, P.J., "Gaussian Basis Sets for Molecular Calculations," Modern Theoretical Chemistry, Methods of Electronic Structure Theory, Vol. 3, H.F. Schaefer, III, ed., Plenum, New York, 1977.

36. Benioff, P.A., "Ab Initio Calculations of the Vertical Eletronic Spectra of NO_2, NO_2^+, and NO_2^-," J. Chem. Phys., Vol. 68, p. 3405, 1978.

37. Almlof, J., in Proceedings of the 2nd Seminar on Computational Problems in Chemistry, Strausbourg, France, 1972, published 1973.

38. Kormornicki, A., National Resource for Computations in Chemistry Software Catalog, Vol. 1, Program No. QH04(GRADSCF), 1980.

39. Hariharan, P.C., and Pople, J.A., "Accuracy of AH_m Equilibrium Geometries by Single Determinant Molecular Orbital Theory," Mol. Phys., Vol. 27, p. 209, 1974.

40. **Seery, D.J., and Bowman, C.T., "An Experimental and Analytical Study of** Methane Oxidation Behind Shock Waves," Combustion and Flame, Vol. 14, p. 37, 1970.

41. **McKellar, J.F., and Norrish, R.G.W., "The Combustion of Gaseous Aldehydes** Studied by Flash Photolysis and Kinetic Spectroscopy," Proc. Roy. Soc. Lond., Ser. A, Vol. 254, p. 147, 1960.

42. **Westbrook, C.K., Creighton, J., Lund, C., and Dryer, F.L., "A Numerical Model** of Chemical Kinetics of Combustion in a Turbulent Flow Reactor," J. Phys. Chem., Vol. 81, p. 2542, 1977.

43. **Botschwina, P., "Unrestricted Hartree-Fock Calculation of Force Constants** and Vibrational Frequencies of the HCO Molecule," Chem. Phys. Lett., Vol. 29, p. 98, 1974.

44. **Cremaschi, P., Gamba, A., Morosi, G., and Simonetta, M., "Influence of Spin-**Contamination and Basis Set on Electrostatic Potential and hfs Coupling Constants of Organic Radicals," Theoret. Chim. Acta, Vol. 41, p. 177, 1976.

45. **Bruna, P.J., Buenker, R.J., and Peyerimhoff, S.D., "Ab Initio Study of the** Structure, Isomers, and Vertical Electronic Spectrum of the Formyl Radical, HCO," J. Mol. Struct., Vol. 32, p. 217, 1976.

46. **Dunning, T.H., "Theoretical Characterization of the Potential Energy** Surface of the Ground State of the HCO System," J. Chem. Phys., Vol. 73, p. 2304, 1980.

47. **Brown, J.M., and Ramsay, D.A., "Axis Switching in the $\tilde{A}\ ^2A''$-$\tilde{X}^2A'$ Transition** of HCO: Determination of Molecular Geometry," Can. J. Phys., Vol. 53, p. 2232, 1975.

48. **Warneck, P., "Photoionisation von Methanol und Formaldehyd,** Z Naturforsch., Vol. A29, p. 350, 1974.

49. **Wang, H.Y., Eyre, J.A., and Dorfman, L.M., "Activation Energy for the Gas-**Phase Reaction of Hydrogen Atoms with Carbon Monoxide," J. Chem. Phys., Vol. 59, p. 5199, 1973.

50. **Milligan, D.E., and Jacox, M.E., "Matrix Isolation Study of the Infrared and** Ultraviolet Spectra of the Free Radical HCO. The Hydrocarbon Flame Bands," J. Chem. Phys., Vol. 51, p. 277, 1969.

51. **Reilly, J.P., Clark, J.H., Moore, C.B., and Pimental, G.C., "HCO Production,** Vibrational Relaxation, Chemical Kinetics, and Spectroscopy Following Laser Photolysis of Formaldehyde," J. Chem. Phys., Vol. 69, p. 4381, 1978.

52. **Johns, J.W.C., McKellar, A.R.W., and Riggen, M., "Laser Magnetic Resonance** Spectroscopy of the ν_2 Band of HCO at 9.25 μm," J. Chem. Phys., Vol. 67, p. 2323, 1977.

53. Rosenberg, B.J., Ermler, W.C., and Shavitt, I., "Ab Initio SCF and CI Studies on the Ground State of the Water Molecule. II. Potential Energy and Property Surfaces," J. Chem. Phys., Vol. 65, p. 4072, 1976.

54. Clyne, M.A.A., and Thrush, B.A., "Mechanism of Chemiluminescent Reactions Involving Nitric Oxide - The H + NO Reaction," Disc. Faraday Soc., Vol. 33, p. 139, 1962.

55. Salotto, A.W., and Burnelle, L., "Investigations on the Unrestricted Hartree-Fock Method as a Tool for Computing Potential Energy Surfaces," J. Chem. Phys., Vol. 52, p. 2936, 1970.

56. Wu, A.A., Peyerimhoff, S.D., and Buenker, R.J., "Theoretical Study of the Electronic Spectrum of HNO Using SCF and CI Calculations," Chem. Phys. Lett., Vol. 35, p. 316, 1975.

57. Freedman, P.A., "Predissociation in the HNO Molecule," Chem. Phys. Lett., Vol. 44, p. 605, 1976.

58. Cashion, J.K, and Polanyi, J.C., "Infrared Chemiluminescence from the Gaseous Reaction of Atomic H Plus NO; HNO in Emission," J. Chem. Phys., Vol. 30, p. 317, 1959.

59. Clement, M.J.Y., and Ramsay, D.A., "Predissociation in the HNO Molecule," Can. J. Phys., Vol. 39, p. 205, 1961.

60. Clyne, M.A.A., and Thrush, B.A., "Reaction of Hydrogen Atoms with Nitric Oxide," Trans. Faraday Soc., Vol. 57, p. 1305, 1961.

61. Krauss, M., "Test of a Kinetics Scheme: Emission in $H(^2S) + NO(^2\Pi)$. J. Res. Natl. Bur. Std., Vol. 73A, p. 191, 1969.

62. Nomura, O., and Iwato, S., "Potential Energy Curves for Low-Lying States of HNO," Chem. Phys. Lett., Vol. 66, p. 523, 1979.

63. Dalby, F.W., "The Spectrum and Structure of the HNO Molecule," Can. J. Phys., Vol. 36, p. 1336, 1958.

64. Bancroft, J.L., Hollas, J.M., and Ramsay, D.A., "The Absorption Spectrum of HNO and DNO," Can. J. Phys., Vol. 40, p. 322, 1962.

65. Ishiwata, T., Akimoto, H., and Tanaka, I., "Chemiluminescence of HNO Sensitized by $O_2(^1\Delta_g)$ in the Reaction Systems of $O(^3P) + C_3H_6 + NO + O_2(^1\Delta_g)/O_2$ and $H + NO + O_2(^1\Delta_g)/O_2$," Chem. Phys. Lett., Vol. 27, p. 260, 1974.

66. Ishiwata, T., Tanaka, I., and Akimoto, H., "Excitation of HNO by $O_2(^1\Delta_g)$," J. Phys. Chem., Vol. 82, p. 1336, 1978.

67. Williams, G.R., "A Theoretical Study of the Excited States of the Nitroxyl Radical (HNO) via the Equations of Motion Method," Chem. Phys. Lett., Vol. 30, p. 495, 1975.

68. Wu, A.A., Peyerimhoff, S.D., and Buenker, R.J., "Theoretical Study of the Electronic Spectrum of HNO Using SCF and CI Calculations," Chem. Phys. Lett., Vol. 35, p. 315, 1975.

69. Huber, K.P., and Herzberg, G., Molecular Spectra and Molecular Structure. IV. Constants of Diatomic Molecules, Van Nostrand Reinhold, New York, 1979.

70. Adams, G.F., unpublished results.

71. Clough, R.N., Thrush, B.A., Ramsay, D.A., and Stamper, J.G., "The Vibrational Frequencies of HNO," Chem. Phys. Lett., Vol. 23, p. 155, 1973.

72. Johns, J.W.C., and McKellar, A.R.W., "Laser Stark Spectroscopy of the Fundamental Bands of HNO (ν_2 and ν_3) and DNO (ν_1 and ν_2)," J. Chem. Phys., Vol. 66, p. 1217, 1977.

73. Troe, J., "Theory of Thermal Unimolecular Reactions at Low Pressures. I. Solutions of the Master Equation," J. Chem. Phys., Vol. 66, p. 4745, 1977.

74. Troe, J., "Theory of Thermal Unimolecular Reactions at Low Pressures. II. Strong Collision Rate Constants. Applications," J. Chem. Phys., Vol. 66, p. 4758, 1977.

75. Troe, J., "Predictive Possibilities of Unimolecular Rate Theory," J. Phys. Chem., Vol. 83, p. 114, 1979.

DISTRIBUTION LIST

No. Of Copies	Organization
12	Administrator Defense Technical Info Center ATTN: DTIC-DDA Cameron Station Alexandria, VA 22304-6145
1	HQ DA DAMA-ART-M Washington, DC 20310
1	Commander US Army Materiel Command ATTN: AMCDRA-ST 5001 Eisenhower Avenue Alexandria, VA 22333-0001
10	Central Intelligence Agency Office of Central Reference Dissemination Branch Room GE-47 HQS Washington, DC 20505
1	Commander Armament R&D Center US Army AMCCOM ATTN: SMCAR-TSS Dover, NJ 07801
1	Commander Armament R&D Center US Army AMCCOM ATTN: SMCAR-TDC Dover, NJ 07801
1	Director Benet Weapons Laboratory Armament R&D Center US Army AMCCOM ATTN: SMCAR-LCB-TL Watervliet, NY 12189
1	Commander US Army Armament, Munitions and Chemical Command ATTN: SMCAR-ESP-L Rock Island, IL 61299
1	Commander US Army Aviation Research and Development Command ATTN: AMSAV-E 4300 Goodfellow Blvd. St. Louis, MO 63120
1	Director US Army Air Mobility Research and Development Laboratory Ames Research Center Moffett Field, CA 94035
4	Commander US Army Research Office ATTN: R. Ghirardelli D. Mann R. Singleton R. Shaw P.O. Box 12211 Research Triangle Park, NC 27709-2211
1	Commander US Army Communications - Electronics Command ATTN: AMSEL-ED Fort Monmouth, NJ 07703
1	Commander ERADCOM Technical Library ATTN: DELSD-L, Reports Section Fort Monmouth, NJ 07703-5301
2	Commander Armament R&D Center US Army AMCCOM ATTN: SMCAR-LCA-G, D.S. Downs J.A. Lannon Dover, NJ 07801
1	Commander Armament R&D Center US Army AMCCOM ATTN: SMCAR-LC-G, L. Harris Dover, NJ 07801

DISTRIBUTION LIST

No. Of Copies	Organization
1	Commander Armament R&D Center US Army AMCCOM ATTN: SMCAR-SCA-T, L. Stiefel Dover, NJ 07801
1	Commander US Army Missile Command Research, Development and Engineering Center ATTN: AMSMI-RD Redstone Arsenal, AL 35898
1	Commander US Army Missile and Space Intelligence Center ATTN: AMSMI-YDL Redstone Arsenal, AL 35898-5000
2	Commander US Army Missile Command ATTN: AMSMI-RK, D.J. Ifshin W. Wharton Redstone Arsenal, AL 35898
1	Commander US Army Missile Command ATTN: AMSMI-RKA, A.R. Maykut Redstone Arsenal, AL 35898-5249
1	Commander US Army Tank Automotive Command ATTN: AMSTA-TSL Warren, MI 48397-5000
1	Director US Army TRADOC Systems Analysis Activity ATTN: ATAA-SL White Sands Missile Range, NM 88002
1	Commandant US Army Infantry School ATTN: ATSH-CD-CSO-OR Fort Benning, CA 31905

No. Of Copies	Organization
1	Commander US Army Development and Employment Agency ATTN: MODE-TED-SAB Fort Lewis, WA 98433
1	Office of Naval Research Department of the Navy ATTN: R.S. Miller, Code 432 800 N. Quincy Street Arlington, VA 22217
1	Commander Naval Air Systems Command ATTN: J. Ramnarace, AIR-54111C Washington, DC 20360
2	Commander Naval Ordnance Station ATTN: C. Irish P.L. Stang, Code 515 Indian Head, MD 20640
1	Commander Naval Surface Weapons Center ATTN: J.L. East, Jr., G-23 Dahlgren, VA 22448-5000
2	Commander Naval Surface Weapons Center ATTN: R. Bernecker, R-13 G.B. Wilmot, R-16 Silver Spring, MD 20902-5000
1	Commander Naval Weapons Center ATTN: R.L. Derr, Code 389 China Lake, CA 93555
2	Commander Naval Weapons Center ATTN: Code 3891, T. Boggs K.J. Graham China Lake, CA 93555

DISTRIBUTION LIST

No. Of Copies	Organization
5	Commander Naval Research Laboratory ATTN: M.C. Lin J. McDonald E. Oran J. Shnur R.J. Doyle, Code 6110 Washington, DC 20375
1	Commanding Officer Naval Underwater Systems Center Weapons Dept. ATTN: R.S. Lazar/Code 36301 Newport, RI 02840
1	Superintendent Naval Postgraduate School Dept. of Aeronautics ATTN: D.W. Netzer Monterey, CA 93940
4	AFRPL/DY, Stop 24 ATTN: R. Corley R. Geisler J. Levine D. Weaver Edwards AFB, CA 93523-5000
1	AFRPL/MKPB, Stop 24 ATTN: B. Goshgarian Edwards AFB, CA 93523-5000
1	AFOSR ATTN: J.M. Tishkoff Bolling Air Force Base Washington, DC 20332
1	AFWL/SUL Kirtland AFB, NM 87117
1	Air Force Armament Laboratory ATTN: AFATL/DLODL Eglin AFB, FL 32542-5000
1	NASA Langley Research Center Langley Station ATTN: G.B. Northam/MS 168 Hampton, VA 23365
4	National Bureau of Standards ATTN: J. Hastie M. Jacox T. Kashiwagi H. Semerjian US Department of Commerce Washington, DC 20234
1	OSD/SDIO/UST ATTN: L.H. Caveny Pentagon Washington, DC 20301-7100
1	Aerojet Solid Propulsion Co. ATTN: P. Micheli Sacramento, CA 95813
1	Applied Combustion Technology, Inc. ATTN: A.M. Varney P.O. Box 17885 Orlando, FL 32860
2	Applied Mechanics Reviews The American Society of Mechanical Engineers ATTN: R.E. White A.B. Wenzel 345 E. 47th Street New York, NY 10017
1	Atlantic Research Corp. ATTN: M.K. King 5390 Cherokee Avenue Alexandria, VA 22314
1	Atlantic Research Corp. ATTN: R.H.W. Waesche 7511 Wellington Road Gainesville, VA 22065

DISTRIBUTION LIST

No. Of Copies	Organization
1	AVCO Everett Rsch. Lab. Div. ATTN: D. Stickler 2385 Revere Beach Parkway Everett, MA 02149
1	Battelle Memorial Institute Tactical Technology Center ATTN: J. Huggins 505 King Avenue Columbus, OH 43201
1	Cohen Professional Services ATTN: N.S. Cohen 141 Channing Street Redlands, CA 92373
1	Exxon Research & Eng. Co. Government Research Lab ATTN: A. Dean P.O. Box 48 Linden, NJ 07036
1	Ford Aerospace and Communications Corp. DIVAD Division Div. Hq., Irvine ATTN: D. Williams Main Street & Ford Road Newport Beach, CA 92663
1	General Applied Science Laboratories, Inc. ATTN: J.I. Erdos 425 Merrick Avenue Westbury, NY 11590
1	General Electric Armament & Electrical Systems ATTN: M.J. Bulman Lakeside Avenue Burlington, VT 05401
1	General Electric Company 2352 Jade Lane Schenectady, NY 12309
1	General Electric Ordnance Systems ATTN: J. Mandzy 100 Plastics Avenue Pittsfield, MA 01203
2	General Motors Rsch Labs Physics Department ATTN: T. Sloan R. Teets Warren, MI 48090
2	Hercules, Inc. Allegany Ballistics Lab. ATTN: R.R. Miller E.A. Yount P.O. Box 210 Cumberland, MD 21501
1	Hercules, Inc. Bacchus Works ATTN: K.P. McCarty P.O. Box 98 Magna, UT 84044
1	Honeywell, Inc. Government and Aerospace Products ATTN: D.E. Broden/ MS MN50-2000 600 2nd Street NE Hopkins, MN 55343
1	IBM Corporation ATTN: A.C. Tam Research Division 5600 Cottle Road San Jose, CA 95193
1	IIT Research Institute ATTN: R.F. Remaly 10 West 35th Street Chicago, IL 60616

DISTRIBUTION LIST

No. Of Copies	Organization
2	Director Lawrence Livermore National Laboratory ATTN: C. Westbrook M. Costantino P.O. Box 808 Livermore, CA 94550
1	Lockheed Missiles & Space Co. ATTN: George Lo 3251 Hanover Street Dept. 52-35/B204/2 Palo Alto, CA 94304
1	Los Alamos National Lab ATTN: B. Nichols T7, MS-B284 P.O. Box 1663 Los Alamos, NM 87545
1	National Science Foundation ATTN: A.B. Harvey Washington, DC 20550
1	Olin Corporation Smokeless Powder Operations ATTN: V. McDonald P.O. Box 222 St. Marks, FL 32355
1	Paul Gough Associates, Inc. ATTN: P.S. Gough 1048 South Street Portsmouth, NH 03801
2	Princeton Combustion Research Laboratories, Inc. ATTN: M. Summerfield N.A. Messina 475 US Highway One Monmouth Junction, NJ 08852
1	Hughes Aircraft Company ATTN: T.E. Ward 8433 Fallbrook Avenue Canoga Park, CA 91303
1	Rockwell International Corp. Rocketdyne Division ATTN: J.E. Flanagan/HB02 6633 Canoga Avenue Canoga Park, CA 91304
4	Sandia National Laboratories Combustion Sciences Dept. ATTN: R. Cattolica S. Johnston P. Mattern D. Stephenson Livermore, CA 94550
1	Science Applications, Inc. ATTN: R.B. Edelman 23146 Cumorah Crest Woodland Hills, CA 91364
1	Science Applications, Inc. ATTN: H.S. Pergament 1100 State Road, Bldg. N Princeton, NJ 08540
3	SRI International ATTN: G. Smith D. Crosley D. Golden 333 Ravenswood Avenue Menlo Park, CA 94025
1	Stevens Institute of Tech. Davidson Laboratory ATTN: R. McAlevy, III Hoboken, NJ 07030
1	Textron, Inc. Bell Aerospace Co. Division ATTN: T.M. Ferger P.O. Box 1 Buffalo, NY 14240
1	Thiokol Corporation Elkton Division ATTN: W.N. Brundige P.O. Box 241 Elkton, MD 21921

DISTRIBUTION LIST

No. Of Copies	Organization
1	Thiokol Corporation Huntsville Division ATTN: R. Glick Huntsville, AL 35807
3	Thiokol Corporation Wasatch Division ATTN: S.J. Bennett P.O. Box 524 Brigham City, UT 84302
1	TRW ATTN: M.S. Chou MSR1-1016 1 Parke Redondo Beach, CA 90278
1	United Technologies ATTN: A.C. Eckbreth East Hartford, CT 06108
3	United Technologies Corp. Chemical Systems Division ATTN: R.S. Brown T.D. Myers (2 copies) P.O. Box 50015 San Jose, CA 95150-0015
2	United Technologies Corp. ATTN: R.S. Brown R.O. McLaren P.O. Box 358 Sunnyvale, CA 94086
1	Universal Propulsion Company ATTN: H.J. McSpadden Black Canyon Stage 1 Box 1140 Phoenix, AZ 85029
1	Veritay Technology, Inc. ATTN: E.B. Fisher 4845 Millersport Highway P.O. Box 305 East Amherst, NY 14051-0305

No. Of Copies	Organization
1	Brigham Young University Dept. of Chemical Engineering ATTN: M.W. Beckstead Provo, UT 84601
1	California Institute of Tech. Jet Propulsion Laboratory ATTN: MS 125/159 4800 Oak Grove Drive Pasadena, CA 91103
1	California Institute of Technology ATTN: F.E.C. Culick/ MC 301-46 204 Karman Lab. Pasadena, CA 91125
1	University of California, Berkeley Mechanical Engineering Dept. ATTN: J. Daily Berkeley, CA 94720
1	University of California Los Alamos Scientific Lab. P.O. Box 1663, Mail Stop B216 Los Alamos, NM 87545
2	University of California, Santa Barbara Quantum Institute ATTN: K. Schofield M. Steinberg Santa Barbara, CA 93106
2	University of Southern California Dept. of Chemistry ATTN: S. Benson C. Wittig Los Angeles, CA 90007
1	Case Western Reserve Univ. Div. of Aerospace Sciences ATTN: J. Tien Cleveland, OH 44135

DISTRIBUTION LIST

No. Of Copies	Organization
1	Cornell University Department of Chemistry ATTN: T.A. Cool Baker Laboratory Ithaca, NY 14853
1	Univ. of Dayton Rsch Inst. ATTN: D. Campbell AFRPL/PAP Stop 24 Edwards AFB, CA 93523
1	University of Florida Dept. of Chemistry ATTN: J. Winefordner Gainesville, FL 32611
3	Georgia Institute of Technology School of Aerospace Engineering ATTN: E. Price W.C. Strahle B.T. Zinn Atlanta, GA 30332
1	University of Illinois Dept. of Mech. Eng. ATTN: H. Krier 144MEB, 1206 W. Green St. Urbana, IL 61801
1	Johns Hopkins University/APL Chemical Propulsion Information Agency ATTN: T.W. Christian Johns Hopkins Road Laurel, MD 20707
1	University of Michigan Gas Dynamics Lab Aerospace Engineering Bldg. ATTN: G.M. Faeth Ann Arbor, MI 48109-2140
1	University of Minnesota Dept. of Mechanical Engineering ATTN: E. Fletcher Minneapolis, MN 55455
3	Pennsylvania State University Applied Research Laboratory ATTN: K.K. Kuo H. Palmer M. Micci University Park, PA 16802
1	Polytechnic Institute of NY Graduate Center ATTN: S. Lederman Route 110 Farmingdale, NY 11735
2	Princeton University Forrestal Campus Library ATTN: K. Brezinsky I. Glassman P.O. Box 710 Princeton, NJ 08540
1	Princeton University MAE Dept. ATTN: F.A. Williams Princeton, NJ 08544
1	Purdue University School of Aeronautics and Astronautics ATTN: J.R. Osborn Grissom Hall West Lafayette, IN 47906
1	Purdue University Department of Chemistry ATTN: E. Grant West Lafayette, IN 47906
2	Purdue University School of Mechanical Engineering ATTN: N.M. Laurendeau S.N.B. Murthy TSPC Chaffee Hall West Lafayette, IN 47906
1	Rensselaer Polytechnic Inst. Dept. of Chemical Engineering ATTN: A. Fontijn Troy, NY 12181

DISTRIBUTION LIST

No. Of Copies	Organization
1	Stanford University Dept. of Mechanical Engineering ATTN: R. Hanson Stanford, CA 94305
1	University of Texas Dept. of Chemistry ATTN: W. Gardiner Austin, TX 78712
1	University of Utah Dept. of Chemical Engineering ATTN: G. Flandro Salt Lake City, UT 84112
1	Virginia Polytechnic Institute and State University ATTN: J.A. Schetz Blacksburg, VA 24061
1	Commandant USAFAS ATTN: ATSF-TSM-CN Fort Sill, OK 73503-5600

Aberdeen Proving Ground

Dir, USAMSAA
ATTN: AMXSY-D
AMXSY-MP, H. Cohen
Cdr, USATECOM
ATTN: AMSTE-TO-F
Cdr, CRDC, AMCCOM
ATTN: SMCCR-RSP-A
SMCCR-MU
SMCCR-SPS-IL

USER EVALUATION SHEET/CHANGE OF ADDRESS

This Laboratory undertakes a continuing effort to improve the quality of the reports it publishes. Your comments/answers to the items/questions below will aid us in our efforts.

1. BRL Report Number _____ Date of Report _____

2. Date Report Received _____

3. Does this report satisfy a need? (Comment on purpose, related project, or other area of interest for which the report will be used.) _____

4. How specifically, is the report being used? (Information source, design data, procedure, source of ideas, etc.) _____

5. Has the information in this report led to any quantitative savings as far as man-hours or dollars saved, operating costs avoided or efficiencies achieved, etc? If so, please elaborate. _____

6. General Comments. What do you think should be changed to improve future reports? (Indicate changes to organization, technical content, format, etc.)

CURRENT ADDRESS

Name

Organization

Address

City, State, Zip

7. If indicating a Change of Address or Address Correction, please provide the New or Correct Address in Block 6 above and the Old or Incorrect address below.

OLD ADDRESS

Name

Organization

Address

City, State, Zip

(Remove this sheet along the perforation, fold as indicated, staple or tape closed, and mail.)

FOLD HERE

Director
U.S. Army Ballistic Research Laboratory
ATTN: SLCBR-DD-T
Aberdeen Proving Ground, MD 21005-5066

NO POSTAGE
NECESSARY
IF MAILED
IN THE
UNITED STATES

OFFICIAL BUSINESS
PENALTY FOR PRIVATE USE, $300

BUSINESS REPLY MAIL
FIRST CLASS PERMIT NO 12062 WASHINGTON, DC
POSTAGE WILL BE PAID BY DEPARTMENT OF THE ARMY

Director
U.S. Army Ballistic Research Laboratory
ATTN: SLCBR-DD-T
Aberdeen Proving Ground, MD 21005-9989

FOLD HERE

END

DTIC

8-86